The Astrophysical Journal Letters, 802:L11 (6pp), 2015 March 20 doi:10.1088/2041-8205/802/1/L11
© 2015. The American Astronomical Society. All rights reserved.

MEASURING STAR FORMATION RATES AND FAR-INFRARED COLORS OF HIGH-REDSHIFT GALAXIES USING THE CO(7–6) AND [N II] 205 μm LINES*

Nanyao Lu[1], Yinghe Zhao[1,2,3], C. Kevin Xu[1], Yu Gao[2,3], Tanio Díaz-Santos[4,5], Vassilis Charmandaris[6,7,8], Hanae Inami[9], Justin Howell[1], Lijie Liu[2,10], Lee Armus[4], Joseph M. Mazzarella[1], George C. Privon[11], Steven D. Lord[12], David B. Sanders[13], Bernhard Schulz[1], and Paul P. van der Werf[14]
[1] Infrared Processing and Analysis Center, California Institute of Technology, MS 100-22, Pasadena, CA 91125, USA; lu@ipac.caltech.edu
[2] Purple Mountain Observatory, Chinese Academy of Sciences, Nanjing 210008, China
[3] Key Laboratory of Radio Astronomy, Chinese Academy of Sciences, Nanjing 210008, China
[4] Spitzer Science Center, California Institute of Technology, MS 220-6, Pasadena, CA 91125, USA
[5] Nucleo de Astronomia de la Facultad de Ingenieria, Universidad Diego Portales, Av. Ejercito Libertador 441, Santiago, Chile
[6] Department of Physics, University of Crete, GR-71003 Heraklion, Greece
[7] IAASARS, National Observatory of Athens, GR-15236 Penteli, Greece
[8] Chercheur Associé, Observatoire de Paris, F-75014, Paris, France
[9] National Optical Astronomy Observatory, Tucson, AZ 85719, USA
[10] Max-Planck-Institut für Radioastronomie, Auf dem Hügel 69, D-53121 Bonn, Germany
[11] Departamento de Astronomía, Universidad de Concepción, Casilla 160 C, Concepción, Chile
[12] The SETI Institute, 189 Bernardo Avenue Suite 100, Mountain View, CA 94043, USA
[13] Institute for Astronomy, University of Hawaii, 2680 Woodlawn Drive, Honolulu, HI 96822, USA
[14] Leiden Observatory, Leiden University, P.O. Box 9513, 2300 RA Leiden, The Netherlands
Received 2015 January 22; accepted 2015 March 6; published 2015 March 23

ABSTRACT

To better characterize the global star formation activity in a galaxy, one needs to know not only the star formation rate (SFR) but also the rest-frame, far-infrared color (e.g., the 60–100 μm color, C(60/100)) of the dust emission. The latter probes the average intensity of the dust heating radiation field and scales statistically with the effective SFR surface density in star-forming galaxies including (ultra-)luminous infrared galaxies ((U)LIRGs). To this end, here we exploit a new spectroscopic approach involving only two emission lines: CO(7–6) at 372 μm and [N II] at 205 μm([N II]$_{205\mu m}$). For local (U)LIRGs, the ratios of the CO(7–6) luminosity ($L_{\rm CO(7-6)}$) to the total infrared luminosity ($L_{\rm IR}$; 8–1000 μm) are fairly tightly distributed (to within ∼0.12 dex) and show *little* dependence on C(60/100). This makes $L_{\rm CO(7-6)}$ a good SFR tracer, which is less contaminated by active galactic nuclei than $L_{\rm IR}$ and may also be much less sensitive to metallicity than $L_{\rm CO(1-0)}$. Furthermore, the logarithmic [N II]$_{205\mu m}$/CO(7–6) luminosity ratio depends fairly strongly (at a slope of ∼−1.4) on C(60/100), with a modest scatter (∼0.23 dex). This makes it a useful estimator on C(60/100) with an implied uncertainty of ∼0.15 (or $\lesssim$4 K in the dust temperature ($T_{\rm dust}$) in the case of a graybody emission with $T_{\rm dust} \gtrsim 30$ K and a dust emissivity index $\beta \geqslant 1$). Our locally calibrated SFR and C(60/100) estimators are shown to be consistent with the published data of (U)LIRGs of z up to ∼6.5.

Key words: galaxies: active – galaxies: ISM – galaxies: star formation – infrared: galaxies – ISM: molecules – submillimeter: galaxies

1. INTRODUCTION

Luminous infrared galaxies (LIRGs: with an 8–1000 μm $L_{\rm IR} > 10^{11}\,L_\odot$; Sanders & Mirabel 1996), including ultra-luminous ones (ULIRGs, $L_{\rm IR} > 10^{12}\,L_\odot$), dominate the cosmic star formation (SF) at $z \gtrsim 1$ (e.g., Le Flóch et al. 2005). For z ∼ 1 to 3, these galaxies are mixtures of two populations based on their prevalent "SF mode": (a) mergers dominated by nuclear starburst with warm far-infrared (FIR) colors and a high SF efficiency (SFE) similar to that in local ULIRGs, and (b) gas-rich disk galaxies with disk SF and SFE comparable to local spirals (e.g., Daddi et al. 2010); more ULIRGs belong to the latter "main-sequence" (MS) population (e.g., Elbaz et al. 2011). However, the current perception that the typical spectral energy distribution (SED) of the dust emission in the high-z, MS galaxy population is merely a "scaled-up" SED of local normal galaxies remains unproven: if the size of the effective SF region in a galaxy is fixed, an increasing $L_{\rm IR}$ implies a higher effective star formation rate (SFR) surface density ($\Sigma_{\rm SFR}$), which is known to lead to a warmer FIR color or the 60-to-100 μm flux density ratio, C (60/100) (thus, the SED shape) for both normal galaxies and (U)LIRGs (Chanial et al. 2007; Liu et al. 2015). As demonstrated by Rujopakarn et al. (2011), the high-z (U)LIRGs from the MS population are comparable in size to the local star-forming galaxies, but with a much higher $\Sigma_{\rm SFR}$. In general, C(60/100) probes the average intensity of the dust heating radiation field (e.g., Draine & Li 2007), and both SFR and C(60/100) should be measured in order to more fully characterize the SF activity in galaxies.

The conventional way to do so is to obtain a full dust SED from which both the SFR (from $L_{\rm IR}$) and C(60/100) can be deduced. For high-z galaxies, this usually requires multiple photometric measurements covering a wide wavelength range, as illustrated in the recent studies on 3 galaxies at z ∼ 5–6 (Riechers et al. 2013; Gilli et al. 2014; Rawle et al. 2014). Furthermore, as z increases, accurate continuum photometry becomes tougher due to relatively bright background. A promising alternative is to measure SFR and C(60/100) using spectral lines in the FIR/sub-millimeter. A recent spectroscopic

* Based on *Herschel* observations. *Herschel* is an ESA space observatory with science instruments provided by European-led Principal Investigator consortia and with important participation from NASA.

survey with the *Herschel Space Observatory* (*Herschel*) on a large sample of LIRGs from the Great Observatories All-Sky LIRG Survey (GOALS; Armus et al. 2009) revealed a remarkable one-to-one relation between the luminosity summed over the CO rotational transitions in the mid-J regime ($5 \leqslant J \lesssim 10$) and $L_{\rm IR}$ (Lu et al. 2014, hereafter Paper I). Here we exploit the method of using only the CO(7–6) line luminosity, $L_{\rm CO(7-6)}$, as an SFR tracer. Furthermore, we show that, for the local (U)LIRGs, the [N II] 205 μm line (hereafter referred to as [N II]) to CO(7–6) flux ratio is fairly steeply correlated with C(60/100) with a modest scatter. As a result, it can serve as a useful estimator of C(60/100).

In the remainder of this Letter, we describe the galaxy samples and data used in Section 2, present our analysis and results in Section 3, and compare our results to the existing observations of distant galaxies in Section 4.

2. DATA SAMPLES

2.1. Local LIRGs

Paper I described a *Herschel* spectroscopic survey of a flux-limited set of 125 LIRGs from GOALS using the Spectral and Photometric Imaging REceiver (SPIRE; Griffin et al. 2010). While the detailed data will be presented elsewhere (Lu et al., in preparation), the measured CO and [N II] fluxes based on the point-source flux calibration, as described in Paper I and Zhao et al. (2013), are used here. The fluxes of the [C II] line at 158 μm (hereafter as [C II]) for our galaxies were taken from Díaz-Santos et al. (2013), obtained with the *Herschel* Photodetector Array Camera and Spectrometer (PACS; Poglitsch et al. 2010). These are also point-source calibrated fluxes, approaching the total flux for sources with a [C II] extent not too extended relative to the PACS beam of $\sim$12″ (FWHM).

For each GOALS galaxy, the [Ne V] 14.3 μm to [Ne II] 12.8 μm line ratio (hereafter [Ne V]/[Ne II]) or its upper limit is available in Inami et al. (2013). Five galaxies in our GOALS/SPIRE sample have [Ne V]/[Ne II] >0.65, for which the active galactic nucleus (AGNs) contribution to the total bolometric luminosity is likely greater than 50% (Farrah et al. 2007).

2.2. Local ULIRGs

Containing only seven ULIRGs, our GOALS/SPIRE sample covers mainly LIRGs, particularly lower luminosity ones. We also obtained from the *Herschel* archive and reduced in the same way the SPIRE spectroscopic observations of 28 ULIRGs (i.e., the local ULIRG sample), which extend our $L_{\rm IR}$ coverage to $\sim 10^{13}\,L_{\odot}$. These observations were performed in the program "OT1_dfarrah_1" (PI: D. Farrah). For many of these galaxies, the [C II] fluxes are available from Farrah et al. (2013). Only one galaxy in this sample has [Ne V]/[Ne II] >0.65 (Farrah et al. 2007).

2.3. Local Dwarf Galaxies

Our GOALS/SPIRE sample also includes one blue compact dwarf, Haro 11, with a metallicity $Z \approx 0.45\,Z_{\odot}$, where $Z_{\odot} = (12 + \log {\rm O/H})_{\rm solar} = 8.7$ (Asplund et al. 2009). We obtained archival SPIRE spectra on three additional dwarfs: NGC 4214 ($Z \sim 0.36\,Z_{\odot}$; obsid = 1342256082; Madden et al. 2013), IC 10 ($\sim$0.29 $Z_{\odot}$; 1342246982) and He 2–10 ($\sim$0.54 $Z_{\odot}$; 1342245083) (PI: V. Lebouteiller). The metallicity values were taken from Rémy-Ruyer et al. (2013). Both IC 10 and NGC 4214are extended and their SPIRE observations were pointed at the brightest H II region. We extracted a CO(7–6) flux from the point-source calibrated spectrum of the central detector. The corresponding $f_{\nu}(70\,\mu{\rm m})$ and $f_{\nu}(100\,\mu{\rm m})$ were derived by convolving the SPIRE beam of CO(7–6) with the corresponding PACS images (Rémy-Ruyer et al. 2013) and used to calculate the FIR luminosity ($L_{\rm FIR}$; Helou et al. 1985) after inferring $f_{\nu}(60\,\mu{\rm m})$ from a matching FIR model SED from Dale et al. (2001). He 2–10 is infrared compact (Bendo et al. 2012). Its SPIRE observation is a map. We therefore extracted from the map a point-source spectrum at the location of the peak brightness using the task "specPointSourceExtractor" in the *Herschel* Interactive Processing Environment software (HIPE). The extracted spectrum was further corrected for an optimized source extent of 18″ (Gaussian FWHM) using the HIPE semi-extended source correction tool (Wu et al. 2013) before extracting our CO(7–6) and [N II] fluxes. Finally, the total [C II] flux of He 2–10 was taken from Cormier et al. (2015).

3. ANALYSIS

3.1. CO(7–6) as an SFR Tracer

We used the PACS 70 μm continuum images of J. Chu et al. (2015, in preparation) to select only those GOALS galaxies that are not too extended with respect to the SPIRE beam, which measures (FWHM) 35″ and 17″ for CO(7–6) and [N II], respectively, in order to use the point-source calibrated fluxes. For each galaxy, we calculated $f_{70\,\mu{\rm m}}(\theta)$, the fractional 70 μm flux within a Gaussian beam of FWHM θ. The CO(7–6) and [N II] analyses here are further limited to those GOALS galaxies satisfying $f_{70\,\mu{\rm m}}(30'') > 85\%$ (102 galaxies; the average value of $f_{70\,\mu{\rm m}}(30'') = 97\%$) and $f_{70\,\mu{\rm m}}(17'') > 70\%$ (98 galaxies; the average value = 89%), respectively. These were chosen so that at least 75% of the GOALS galaxies in the coldest FIR color ($0.45 \lesssim C\,(60/100) \leqslant 0.6$) or smallest $L_{\rm IR}$ ($11 \lesssim \log L_{\rm IR}/L_{\odot} \leqslant 11.3$) bin meet the criterion, and that any systematic effect from the possible aperture flux loss is significantly smaller than the sample scatter in the flux ratios dealt with here.

In Figure 1 we plot both $L_{\rm CO(7-6)}/L_{\rm IR}$ and $L_{\rm CO(7-6)}/L_{\rm FIR}$ as a function of C(60/100) for the local galaxies. The AGNs with [Ne V]/[Ne II] $>$ 0.65 are further circled. For IC 10 and NGC 4214, we could only obtain their $L_{\rm FIR}$. As a result, they are only shown in Figure 1(b).

NGC 6240 is a rare outlier with additional gas heating likely from shocks unrelated to the ongoing SF (see Paper I). The AGNs in Figure 1 have a lower CO/IR ratio on average. This is more apparent in CO(7–6)/IR than in CO(7–6)/FIR, consistent with that the lower CO/IR ratio in an AGN is mostly due to the AGN "contamination" to $L_{\rm IR}$ (see Paper I). In this sense, CO(7–6) is a "cleaner" SFR tracer than $L_{\rm IR}$.

A galactic CO spectral line energy distribution (SLED) generally consists of up to three distinct gas components, which dominate the SLED at the low (i.e., $J \lesssim 4$), mid ($\sim$5 to $\sim$10) and high J (>10) regimes, respectively; the mid-J component is directly related to the ongoing SF (see Paper I; Xu et al. 2015). On either side (in J) of this SF-driven component, the "contamination" from one of the other gas components increases. We found that CO(7–6) traces $L_{\rm IR}$ better than any other mid-J CO line. For example, the CO

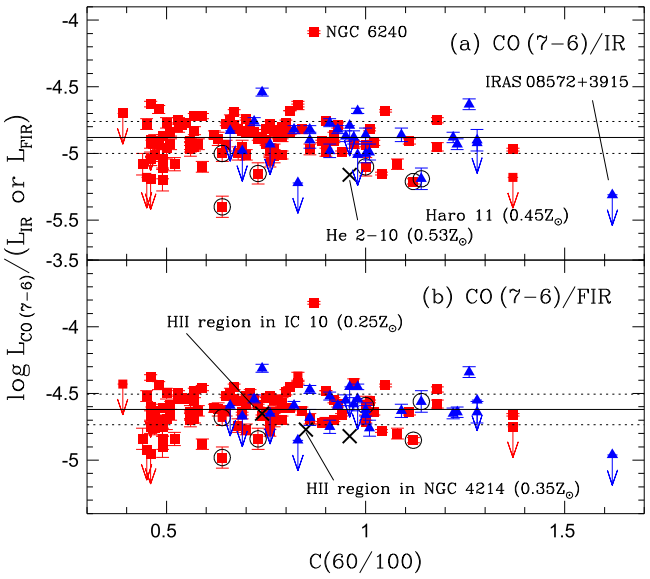

Figure 1. Plots of the logarithmic ratio of $L_{\rm CO(7-6)}$ to $L_{\rm IR}$ in (a) and to $L_{\rm FIR}$ in (b) against C(60/100), for the 102 selected (see the text) GOALS/SPIRE galaxies (red squares) and the local ULIRGs (blue triangles). The error bars shown are at 1σ. The non-detections are shown with their 3σ upper limit. The six powerful AGNs are further enclosed by a circle. A few dwarf galaxies (large black crosses) are individually labeled. The solid line marks the average ($=-4.88\pm0.01$ in (a) or -4.61 ± 0.01 in (b)), which also agrees well with the median, for the combined (U)LIRG samples and the two dashed lines the corresponding sample standard deviation, both determined from the detections only (but excluding NGC 6240 and the six AGNs).

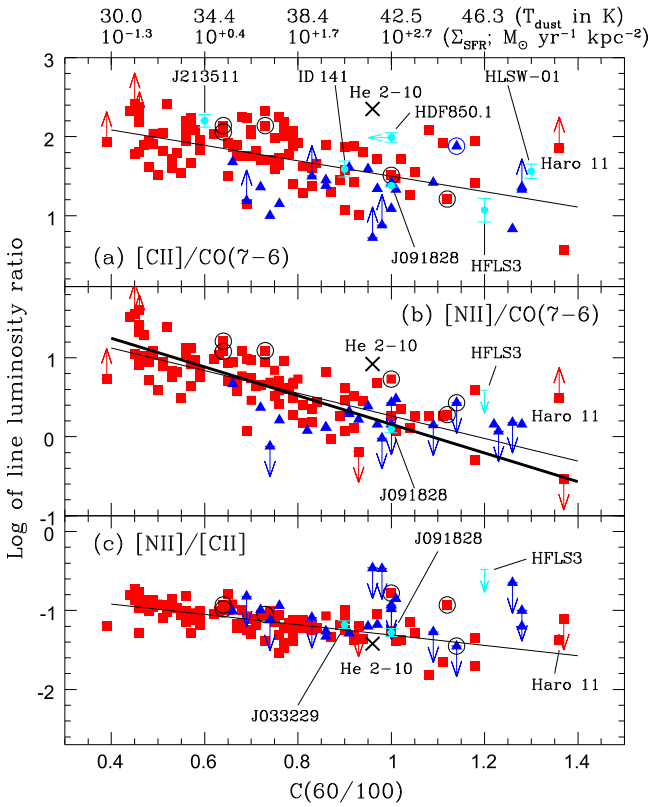

Figure 2. Plots of various line luminosity ratios against C(60/100): (a) [C II] to CO(7–6), (b) [N II] to CO(7–6), and (c) [N II]/[C II], using the same symbols and color schemes as in Figure 1. Only 98 GOALS galaxies are plotted (see the text). The error bars were omitted here as they are smaller than the scatter. The thin solid line indicates a vertical least-squares fit to all the detections of the local (U)LIRGs. The thick solid line in (b) shows the result from a least-squares bisector fit. The AGNs were excluded from these fits. Also shown in cyan and labeled individually are a few high-z galaxies from Table 1, with C(60/100) estimated from the published SEDs. The $T_{\rm dust}$ and $\Sigma_{\rm SFR}$ marks at the top of the plots are explained in the text.

(6–5)/IR ratios from our sample show a small anti-correlation with C(60/100), implying a systematic ratio variation of ~0.29 dex over $0.4 < C(60/100) < 1.3$.

The average CO(7–6)/IR ratio in Figure 1 (i.e., the solid line) can be used to derive an SFR from $L_{\rm CO(7-6)}$ using the SFR-$L_{\rm IR}$ calibration from Kennicutt (1998). Equation (1) gives the results, with the quoted uncertainty being the sample standard deviation ($\sigma_s \approx 0.12$ dex). Since $\sigma_s \approx 0.10$ dex when the total flux of all the mid-J CO lines was used (see Paper I), it is ~5% less accurate when using the CO(7–6) line alone to predict $L_{\rm IR}$:

$$\begin{aligned}{\rm SFR}\Big/\Big(M_\odot\ {\rm yr}^{-1}\Big) &= 1.73\times10^{-10}\Big(L_{\rm IR}/L_\odot\Big)\\ &= 1.31\times10^{-5.00\pm0.12}\Big(L_{\rm CO(7-6)}/L_\odot\Big). \quad (1)\end{aligned}$$

Many local dwarf galaxies with $Z \lesssim 0.5\ Z_\odot$ are relatively faint in CO(1–0), with a CO(1–0)/IR ratio being 1–2 orders of magnitude less than that for normal spirals (e.g., Schruba et al. 2012). This is usually attributed to a more severe CO dissociation by UV photons because of a lower dust opacity. Nevertheless, the mid-J CO line emission arises from dense molecular clouds; possible UV self-shielding (Lee et al. 1996) implies that CO(7–6)/IR should not be as severely dependent on metallicity as CO(1–0)/IR. In Figure 1, both Haro 11 and He 2–10 appear to have somewhat lower flux ratios of CO(7–6) to IR or FIR. On the other hand, the bright H II regions in IC 10 and NGC 4214 are not much different from the (U)LIRGs in terms of the CO (7–6)/FIR ratio. Therefore, the low-metallicity dwarf galaxies examined here show only a moderately lower CO (7–6)/FIR ratio on average, but still within $\sim 2\,\sigma_s$ of the average ratio for the (U)LIRGs.

3.2. [C II]/CO(7–6), [N II]/CO(7–6), and C(60/100)

In Figure 2 we plot the [C II]/CO(7–6), [N II]/CO(7–6) and [N II]/[C II] luminosity ratios as a function of C(60/100) for the local (U)LIRGs. All the plots span 2.3 dex vertically for direct comparison. The dust temperature, $T_{\rm dust}$, and $\Sigma_{\rm SFR}$ marks at the top of the plots were derived respectively from C(60/100) assuming a dust emissivity index of $\beta = 1.5$ and from Equation (2), which represents a least-squares bisector (Isobe et al. 1990) result on a sample of 175 local star-forming galaxies (including 66 (U)LIRGs) in Liu et al. (2015) with $L_{\rm IR}$-based $\Sigma_{\rm SFR}$ and $0.25 \leqslant C(60/100) \lesssim 1.1$. As in Chanial et al. (2007), both the normal galaxies and (U)LIRGs in this sample follow a single trend continuously. However, the rms scatter at a given C(60/100) is still significant, up to ~0.9 dex. Moreover, Equation (2) is calibrated up to $C(60/100) \sim 1.1$:

$$\begin{aligned}&\log \Sigma_{\rm SFR}\Big/\Big(M_\odot\ {\rm yr}^{-1}\,{\rm kpc}^{-2}\Big)\\ &= (10.09\ \pm\ 0.46)\log C(60/100)\ +\ (2.68\ \pm\ 0.17). \quad (2)\end{aligned}$$

The data trends in Figures 2(a) and (b) remain unchanged if $L_{\rm IR}$ or $L_{\rm FIR}$ replaces $L_{\rm CO(7-6)}$. All the three line ratios are anti-correlated with C(60/100). Equations (3)–(5)give the results from a vertical linear regression (i.e., the thin solid lines in Figure 2) using the local (U)LIRG detections in each plot (after excluding the AGNs, but including NGC 6240 that

Table 1
High-redshift Galaxies

Galaxy (1)	z (2)	Type (3)	CO(7–6)/FIR[a,b] (4)	[C II]/CO(7–6)[a] (5)	[N II]/CO(7–6)[a] (6)	[N II]/[C II][a] (7)	C(60/100)[c] (8)	References[d] (9)
IRAS F10214+4724	2.286	QSO	−5.00(0.10)	···	···	···	···	(1, 1, –, –, –)
SMM J213511–0102	2.32	SMG	−4.81(0.02)	2.20(0.08)	···	···	0.6	(2, 2, 3, –, 3)
SMM J16365+4057	2.383	SMG	−4.19(0.04)	···	···	···	···	(2, 2, –, –, –)
SMM J16358+4105	2.452	SMG	−4.36(0.06)	···	···	···	···	(2, 2, –, –, –)
SMM J04431+0210	2.509	SMG	−5.10(0.11)	···	···	···	···	(2, 2, –, –, –)
Cloverleaf	2.558	QSO	−4.20(0.07)	···	···	···	···	(1, 1, –, –, –)
SMM J14011+0252	2.565	SMG	−4.77(0.06)	···	···	···	···	(1, 1, –, –, –)
VCV J1409+5628	2.583	QSO	−4.95(0.08)	···	···	···	···	(1, 1, –, –, –)
AMS12	2.767	QSO	−4.99(0.05)	···	···	···	···	(2, 2, –, –, –)
RX J0911+0551	2.796	QSO	−4.68(0.03)	···	···	···	···	(2, 2, –, –, –)
HLSW-01	2.957	SMG	−4.52(0.05)	1.56(0.09)	···	···	1.3	(2, 2, 4, –, 4)
MM18423+5938	3.930	SMG	−4.87(0.05)	···	0.53(0.02)	···	···	(2, 2, –, 2, –)
SMM J123711+6222	4.055	SMG	−4.71(0.05)	···	···	···	0.9	(2, 5, –, –, 6)
ID 141	4.243	SMG	−4.73(0.04)	1.59(0.10)	···	···	0.9	(2, 2, 7, –, 7)
BR 1202–0725 (N)	4.69	SMG	−4.12(0.05)	1.05(0.08)	<0.50(n/a)	<–0.44(n/a)	···	(2, 8, 9, 10, –)
BR 1202–0725 (S)	4.69	QSO	−4.60(0.04)	1.00(0.07)	<0.04(n/a)	<–0.79(n/a)	···	(2, 8, 9, 10, –)
LESS J033229–2756	4.755	SMG	···	···	···	−1.18(0.05)	0.9	(–, –, 11, 2, 12)
HDF850.1	5.183	SMG	−4.74(0.06)	1.99(0.06)	···	···	$\lesssim$1.0	(2, 13, 14, –, 14)
HLS J091828+5142	5.243	SMG	−4.46(0.02)	1.38(0.02)	0.10(0.05)	−1.28(0.05)	1.0	(15, 15, 15, 15, 15)
HFLS3	6.34	SMG	−4.34(0.10)	1.07(0.15)	<0.59(n/a)	<–0.48(n/a)	1.2	(16, 16, 16, 16, 16)
SDSS J1148+5251	6.419	QSO	−4.61(0.05)	1.16(0.06)	<0.13(n/a)	<–1.03(n/a)	···	(2, 2, 17, 17, –)

[a] Logarithmic luminosity ratios with the 1σ uncertainty in parentheses.
[b] The quoted uncertainty does not include the (likely significant) error in $L_{\rm FIR}$.
[c] C(60/100) estimated from the literature SED fit of a moderate to good quality.
[d] Reference indices for the FIR, CO(7–6), [C II] and [N II] fluxes, and C(60/100), respectively, where the indices refer to the following: (1) see Solomon & Vanden Bout (2005) for the original reference, (2) see Carilli & Walter (2013) for the original reference, (3) Ivison et al. (2010), (4) Magdis et al. (2014), (5) Carilli et al. (2010), (6) Tan et al. (2014), (7) Cox et al. (2011), (8) Salomé et al. (2012), (9) Carilli et al. (2013), (10) Decarli et al. (2014a), (11) De Breuck et al. (2014), (12) Gilli et al. (2014), (13) Decarli et al. (2014b), (14) Walter et al. (2012), (15) Rawle et al. (2014), (16) Riechers et al. (2013), and (17) Walter et al. (2009).

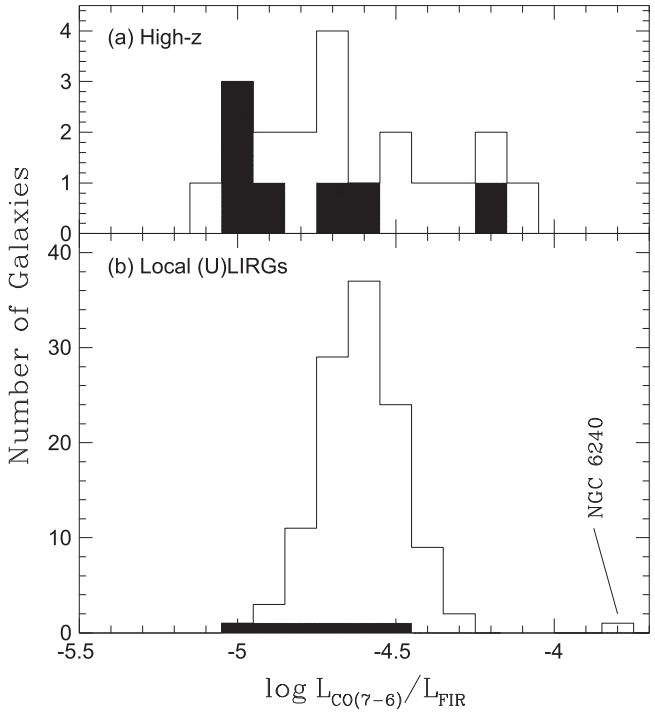

Figure 3. Histograms of log $L_{\rm CO(7-6)}/L_{\rm FIR}$, separately for (a) the high-z sample and (b) our local (U)LIRG galaxies from Figure 1(b). In panel (a), the shaded part represents the QSOs; in (b), the six powerful AGNs are further shaded.

behaves "normally" here). The resulting σ_s with respect to the fit are 0.30, 0.23, and 0.15 dex, respectively. If we had further limited the GOALS galaxies to a subset of 69 galaxies with $f_{70\,\mu{\rm m}}(17'') > 85\%$, the resulting fit would be similar. As demonstrated in Zhao et al. (2013), at a given C(60/100), the scatter in the [N II]/FIR (thus, [N II]/CO(7–6)) flux ratios for SF-dominated galaxies is largely driven by the hardness of the underlying radiation field. The reduced scatter in the [N II]/[C II] ratios suggests that a major part of the scatter in the [C II]/CO(7–6) ratios should also be driven by the radiation hardness:

$$\log\,[{\rm C\,II}]/{\rm CO}(7-6) = (-0.98 \pm 0.14)\,C(60/100) + (2.47 \pm 0.11). \quad (3)$$

$$\log\,[{\rm N\,II}]/{\rm CO}(7-6) = (-1.43 \pm 0.12)\,C(60/100) + (1.69 \pm 0.09). \quad (4)$$

$$\log\,[{\rm N\,II}]/[{\rm C\,II}] = (-0.65 \pm 0.08)\,C(60/100) - (0.66 \pm 0.06). \quad (5)$$

A useful application of Figure 2 at high z is to infer C(60/100) by measuring two of the three lines. Given its stronger dependence upon C(60/100) and modest sample scatter (~0.23 dex), the [N II]/CO(7–6) ratio is the preferred one. While Equation (4) is suitable for inferring the [N II]/CO(7–6) ratio from a measured C(60/100), the reverse inference normally requires a regression of C(60/100) on [N II]/CO(7–6), of which the slope might be biased somewhat due to the selection effect that, at the low C(60/100) end, our LIRG luminosity cutoff may have left out some FIR-colder galaxies at a fixed [N II]/CO(7–6)

ratio. As a compromise, the thick solid line in Figure 2(b) or Equation (6) gives the least-squares bisector result as our favored estimator for $C(60/100)$:

$$C(60/100) = (-0.55 \pm 0.04) \log [\mathrm{N\,II}]/\mathrm{CO}(7-6) + (1.09 \pm 0.03). \quad (6)$$

The resulting scatter in $C(60/100)$ relative to the fit is ∼0.15, equivalent to an accuracy of $\lesssim$4 K in $T_{\rm dust}$ in the case of a graybody emission with $T_{\rm dust} \gtrsim 30$ K and a dust emissivity index $\beta \geqslant 1$. However, it should be noted that Equations (3)–(5) are applicable only for $C(60/100) \gtrsim 0.4$, below which the [N II]/IR trend flattens out (Zhao et al. 2013). Figure 2 also hints that either a strong AGN or a low metallicity might enhance [N II]/CO(7–6) and/or [C II]/CO(7–6). While more data are needed to confirm these possible systematics, it has been known that a low metallicity tends to increase [C II]/FIR (e.g., Madden et al. 1997).

4. APPLICATION TO HIGH-z GALAXIES

Table 1 lists the high-z galaxies with either a CO(7–6) flux or both [C II] and [N II] observations in the literature. They consist of 14 sub-millimeter selected galaxies (SMGs) and 7 quasars (QSOs). The line luminosities in solar units were derived using the formulae in Solomon & Vanden Bout (2005).

There is a considerable uncertainty as to whether an IR luminosity given in the literature for a high-z galaxy is $L_{\rm IR}$ or $L_{\rm FIR}$. When this distinction is not clear, the IR luminosity was usually either derived from a FIR-radio correlation or scaled from a sub-millimeter flux density (see Carilli & Walter 2013), and is therefore closer to $L_{\rm FIR}$ than $L_{\rm IR}$. We therefore compare in Figure 3 the CO(7–6)/FIR ratios between the local (U)LIRGs from Figure 1 and the high-z sample. Considering the small sample size and the fact that the high-z galaxies likely have a much larger error in their $L_{\rm FIR}$, we focus on the sample average. The $\log L_{\rm CO(7--6)}/L_{\rm FIR}$ averages are (-4.76 ± 0.11), (-4.59 ± 0.08), and (-4.61 ± 0.01) for the high-z QSOs, SMGs and the local (U)LIRGs (excluding NGC 6240), respectively. A Student's t-test, allowing for unequal variances (Press et al. 1992, p. 617), showed an 80% (23%) confidence for the local (U)LIRGs and the high-z SMGs (QSOs) to share the same average CO(7–6)/FIR ratio. The high-z QSOs as a class have a lower average ratio than either the high-z SMGs or the local (U)LIRGs. This is consistent with the sample selections, i.e., the QSOs should have stronger AGNs on average than the SMGs. On the other hand, six out of the seven high-z QSOs possess the $L_{\rm CO(7–6)}/L_{\rm FIR}$ ratios comparable to those of the six local AGNs. This also suggests that the high-z galaxies with the lowest CO/FIR ratios are likely caused by the AGN rather than by a low metallicity.

In Figure 2 we also plotted those high-z galaxies with available $C(60/100)$ in Table 1. They all appear to be consistent with the trends defined by the local (U)LIRGs, with an overall agreement within $\sim 1\sigma_s$ when only the detections are considered. There are three galaxies in Table 1 with at least two of the three line ratios measured, but not $C(60/100)$. In every case, the line ratios are consistent with each other within the context of Figure 2.

Hodge et al. (2015) measured $\Sigma_{\rm SFR} \approx 119\,M_\odot$ yr^{-1} kpc^{-2} in J 123711+6222, comparable to the predicted $\sim 165\,M_\odot$ yr^{-1} kpc^{-2} from our Equation (2). For HFLS3 [$C(60/100) \sim 1.2$], the measured $\Sigma_{\rm SFR} \approx 0.73$–$1.15 \times 10^3\,M_\odot$ yr^{-1} kpc^{-2} (Riechers et al. 2013). Equation (2) is calibrated only up to $C(60/100) \sim 1.1$, at which it predicts a mean $\Sigma_{\rm SFR} \approx 10^3\,M_\odot$ yr^{-1} kpc^{-2}.

Our work here offers a simple, empirical method of using just two spectral lines, CO(7–6) and $[\mathrm{N\,II}]_{205\mu\mathrm{m}}$, to measure both SFR and $C(60/100)$ in (U)LIRGs. Both lines suffer little dust extinction and are among the brightest FIR/sub-millimeter cooling lines, making this method particularly suited for probing the SF activity in high-z galaxies. With a modern interferometric facility such as the Atacama Large Millimeter Array, both lines become observable at $z \gtrsim 0.5$. Thus, this technique enables the simultaneous study of the physical conditions (e.g., size) of the ionized and dense molecular gas (e.g., Xu et al. 2015) as well as the SF activity across a wide redshift range.

This paper benefited from a number of thoughtful comments made by an anonymous referee. Support for this work was provided in part by NASA through an award issued by JPL/Caltech. Y.Z. and Y.G. acknowledge support by NSFC grants No. 11390373 and 11420101002, and CAS pilot-b program No. XDB09000000. T.D.-S. acknowledges support by ALMA-CONICYT No. 31130005.

REFERENCES

Armus, L., Mazzarella, J. M., Evans, A. S., et al. 2009, PASP, 121, 559
Asplund, M., Grevesse, N., Sauval, A. J., & Scott, P. 2009, ARA&A, 47, 481
Bendo, G. J., Galliano, F., & Madden, S. C. 2012, MNRAS, 423, 197
Carilli, C. L., Daddi, E., Riechers, D., et al. 2010, ApJ, 714, 1407
Carilli, C. L., Riechers, D., Walter, F., et al. 2013, ApJ, 763, 120
Carilli, C. L., & Walter, F. 2013, ARA&A, 51, 105
Chanial, P., Flores, H., Guiderdoni, B., et al. 2007, A&A, 462, 81
Cormier, D., Madden, S. C., Lebouteiller, V., et al. 2015, A&A, in press (arXiv:1502.03131)
Cox, P., Krips, M., Neri, R., et al. 2011, ApJ, 740, 63
Daddi, E., Elbaz, D., Walter, F., et al. 2010, ApJL, 714, L118
Dale, D., Helou, G., Contursi, A., Silbermann, N., & Kolhatkar, S. 2001, ApJ, 549, 215
De Breuck, C., Williams, R. J., Swinbank, M., et al. 2014, A&A, 565, A59
Decarli, R., Walter, F., Carilli, C., et al. 2014a, ApJ, 782, 17
Decarli, R., Walter, F., Carilli, C., et al. 2014b, ApJ, 782, 78
Díaz-Santos, T., Armus, L., Charmandaris, V., et al. 2013, ApJ, 774, 68
Draine, B. T., & Li, A. 2007, ApJ, 657, 810
Elbaz, D., Dickinson, M., Hwang, H. S., et al. 2011, A&A, 533, A119
Farrah, D., Bernard-Salas, J., Spoon, H. W. W., et al. 2007, ApJ, 667, 149
Farrah, D., Lebouteiller, V., Spoon, H. W. W., et al. 2013, ApJ, 776, 38
Gilli, R., Norman, C., Vignali, C., et al. 2014, A&A, 562, 67
Griffin, M. J., Abergel, A., Abreu, A., et al. 2010, A&A, 518, L3
Helou, G., Soifer, B. T., & Rowan-Robinson, M. 1985, ApJL, 298, L7
Hodge, J. A., Riechers, D., Decarli, R., et al. 2015, ApJ, 798, 18
Inami, H., Armus, L., Charmandaris, V., et al. 2013, ApJ, 777, 156
Isobe, T., Feigelson, E. D., Akritas, M. G., & Babu, G. J. 1990, ApJ, 364, 104
Ivison, R. J., Swinbank, A. M., Swinyard, B., et al. 2010, A&A, 518, L35
Kennicutt, R. C., Jr. 1998, ARA&A, 36, 189
Le Flóch, E., Papovich, C., Dole, H., et al. 2005, ApJ, 632, 169
Lee, H.-H., Herbst, E., Pineau des Forêts, G., Roueff, E., & le Bourlot, J. 1996, A&A, 311, 690
Liu, L., Gao, Y., & Greve, T. R. 2015, ApJ, in press (arXiv:1502.08001)
Lu, N., Zhao, Y., Xu, C. K., et al. 2014, ApJL, 787, L23 (Paper I)
Madden, S. C., Poglitsch, A., Geis, N., Stacey, G. J., & Townes, C. H. 1997, ApJ, 483, 200
Madden, S. C., Rémy-Ruyer, A., Galametz, M., et al. 2013, PASP, 125, 600
Magdis, G. E., Rigopoulou, D., Hopwood, R., et al. 2014, ApJ, 796, 63
Poglitsch, A., Waelkens, C., Geis, N., et al. 2010, A&A, 518, L2
Press, W. H., Teukolsky, S. A., Vetterling, W. T., & Flannery, B. P. 1992, Numerical Recipes in C (2nd ed.; Cambridge: Cambridge Univ. Press)
Rawle, T. D., Egami, E., Bussmann, R. S., et al. 2014, ApJ, 783, 59
Rémy-Ruyer, A., Madden, S. C., Galliano, F., et al. 2013, A&A, 557, A95
Riechers, D. A., Bradford, C. M., Clements, D. L., et al. 2013, Natur, 496, 329
Rujopakarn, W., Rieke, G. H., Eisenstein, D. J., & Juneau, S. 2011, ApJ, 726, 93

Sanders, D. B., & Mirabel, I. F. 1996, ARA&A, 34, 749
Schruba, A., Leroy, A. K., Walter, F., et al. 2012, AJ, 143, 138
Salomé, P., Guélin, M., Downes, D., et al. 2012, A&A, 545, 57
Solomon, P. M., & Vanden Bout, P. A. 2005, ARA&A, 43, 677
Tan, Q., Daddi, E., Magdis, G., et al. 2014, A&A, 569, A98
Walter, F., Weiß, A., Riechers, D. A., et al. 2009, ApJL, 691, L1
Walter, F., Decarli, R., Carilli, C., et al. 2012, Natur, 486, 233
Wu, R., Polehampton, E. T., Etxaluze, M., et al. 2013, A&A, 556, A116
Xu, C. K., Cao, C., Lu, N., et al. 2015, ApJ, 799, 11
Zhao, Y., Lu, N., Xu, C. K., et al. 2013, ApJL, 765, L13